Published in final edited form as:

Osteoporos Int. 2008 May ; 19(5): 645–652. doi:10.1007/s00198-007-0494-x.

Spinal cord injury causes rapid osteoclastic resorption and growth plate abnormalities in growing rats (SCI-induced bone loss in growing rats)

L. Morse,
Department of Physical Medicine and Rehabilitation, Harvard Medical School and Spaulding Rehabilitation Hospital, 140 The Fenway, Boston, MA 02115, USA

Y. D. Teng,
Department of Physical Medicine and Rehabilitation, Harvard Medical School and Spaulding Rehabilitation Hospital, 140 The Fenway, Boston, MA 02115, USA

Department of Neurosurgery, Harvard Medical School and Brigham and Women's Hospital/ Children's Hospital, Boston, MA, USA

Division of Spinal Cord Injury Research, VA Boston Healthcare System, Boston, MA, USA

L. Pham,
Department of Cytokine Biology, Forsyth Institute, Boston, MA, USA

K. Newton,
Department of Neurosurgery, Harvard Medical School and Brigham and Women's Hospital/ Children's Hospital, Boston, MA, USA

Division of Spinal Cord Injury Research, VA Boston Healthcare System, Boston, MA, USA

D. Yu,
Department of Neurosurgery, Harvard Medical School and Brigham and Women's Hospital/ Children's Hospital, Boston, MA, USA

Division of Spinal Cord Injury Research, VA Boston Healthcare System, Boston, MA, USA

W.-L. Liao,
Department of Physical Medicine and Rehabilitation, Harvard Medical School and Spaulding Rehabilitation Hospital, 140 The Fenway, Boston, MA 02115, USA

Division of Spinal Cord Injury Research, VA Boston Healthcare System, Boston, MA, USA

T. Kohler,
Institute for Biomechanics, ETH Zurich, Zurich, Switzerland

R. Müller,
Institute for Biomechanics, ETH Zurich, Zurich, Switzerland

D. Graves,

Correspondence to: L. Morse, lmorse4@partners.org.

Boston University School of Dental Medicine, Boston, MA, USA

P. Stashenko, and
Department of Cytokine Biology, Forsyth Institute, Boston, MA, USA

R. Battaglino
Department of Cytokine Biology, Forsyth Institute, Boston, MA, USA

L. Morse: lmorse4@partners.org

Abstract

Summary—Spinal cord injury causes severe bone loss. We report osteoclast resorption with severe trabecular and cortical bone loss, decreased bone mineral apposition, and growth plate abnormalities in a rodent model of contusion spinal cord injury. These findings will help elucidate the mechanisms of osteoporosis following neurological trauma.

Introduction—Limited understanding of the mechanism(s) that underlie spinal cord injury (SCI)-induced bone loss has led to few treatment options. As SCI-induced osteoporosis carries significant morbidity and can worsen already profound disability, there is an urgency to advance knowledge regarding this pathophysiology.

Methods—A clinically relevant contusion model of experimental spinal cord injury was used to generate severe lower thoracic SCI by weight-drop (10 g×50 mm) in adolescent male Sprague-Dawley rats. Body weight and gender-matched naïve (no surgery) rats served as controls. Bone microarchitecture was determined by micro-computed tomographic imaging. Mature osteoclasts were identified by TRAP staining and bone apposition rate was determined by dynamic histomorphometry.

Results—At 10 days post-injury we detected a marked 48% decrease in trabecular bone and a 35% decrease in cortical bone at the distal femoral metaphysis by micro-CT. A 330% increase in the number of mature osteoclasts was detected at the growth plate in the injured animals that corresponded with cellular disorganization at the chondro-osseous junction. Appositional growth studies demonstrated decreased new bone formation with a mineralization defect indicative of osteoblast dysfunction.

Conclusions—Contusion SCI results in a rapid bone loss that is the result of increased bone resorption and decreased bone formation.

Keywords

Bone; Osteoclast; Osteoporosis; Rehabilitation medicine; Spinal cord injury

Introduction

Spinal cord injury (SCI) causes severe osteoporosis that increases the risk of low-impact fractures. As a result, up to 70% of all individuals with SCI will fracture spontaneously or in response to minimal trauma at some point following their injury [1]. These fractures can be catastrophic as they limit mobility, worsen disability, interfere with implementation of rehabilitation treatment, and predispose to additional medical complications including

pressure ulcers, osteomyelitis at the fracture site, hypertensive crisis secondary to autonomic dysreflexia, and worsening of functional impairment [2–6].

Clinically, bone loss following SCI is unique in both the severity and pattern of resorption. The most profound bone loss and therefore the skeletal site most frequently fractured is the knee. This is in stark contrast to postmenopausal osteoporosis where clinically relevant bone loss and fractures occur at the hip and lumbar spine. In complete spinal cord injury, bone loss proceeds at a rate of 1% per week for the first 6–12 months [1, 7, 8], a rate that is fourfold greater than that observed during microgravity (0.25%/week) [9] and tenfold greater than following periods of prolonged bed rest (0.1%/week) [10]. At 6 months post-injury, a 40% reduction in total bone mass below the neurological injury can occur [11–15]. By comparison, bone loss in early menopause in the able-bodied is 1.2–1.5% per year [16]. Taken together these findings strongly suggest that SCI-induced bone loss is not solely due to disuse and lack of mobility.

The central nervous system (CNS) is known to be a major regulator of bone metabolism as shown by recent studies that suggest the influence of higher integrating neuronal pathways [17]. Bone is densely innervated, and the observation of direct contact of nerve fibers and bone cells strongly supports a role of innervation in bone cell functions. A number of neuromediators have also been detected by immunocytochemistry in nerve fibers in bone [18–23]. These studies suggest an important role of the neural system in regulating bone cell functions, and ultimately in influencing bone homeostasis.

Experimental contusion injury is a well studied model that is considered to be more physiologic and representative of human SCI pathology than cord transection. It has been used to determine the effects of various treatments on spinal cord recovery [24, 25] as well as to study common sequelae of SCI ranging from neuropathic pain [26, 27] to neurogenic bladder [28, 29]. However, there are no studies of bone loss following contusion injury in rodents. In this study we use the contusion model of spinal cord injury to determine the impact of SCI on bone density, bone microarchitecture, and the bone microenvironment at the distal femoral metaphysis.

Methods

Animals and SCI

Seven-week-old adolescent male Sprague-Dawley (SD) rats (200–225 grams) were anesthetized with i.p. ketamine (75 mg/kg) and xylazine (10 mg/kg). A severe T10 contusion injury was produced utilizing the New York University (NYU) SCI impactor (10 g×50 mm) as previously described [30]. The control group consisted of naïve, age-matched male Sprague Dawley rats. Post-injury care for rats was carried out as we have previously described [30, 31]. Animals were euthanized on day 10 post-injury for subsequent analyses. The Institutional Animal Care and Use Committee at the VA Boston Healthcare System approved all procedures involving animals. We used the Basso, Beattie, Bresnahan (BBB) scale to confirm injury severity by rating hindlimb functional deficits on day 1 and 7 post-injury as previously described [31]. All injured animals demonstrated profound neurological impairment.

In vivo assessment of bone mineral density (BMD)

The femoral metaphysis was chosen for analysis based on the high clinical relevance associated with the fracture frequency at this skeletal site in spinal cord injured individuals. The distal forelimb was chosen as a supralesional control. Prior to sacrifice all animals were anesthetized and bone mineral density was assessed in vivo by PIXImus Scan (Lunar PIXImus2, software version 1.4X). The animals were positioned on their abdomens with the hindlimb externally rotated. The hip and knee were flexed to 110 degrees with the ankle in neutral position. The forelimb was externally rotated. Two regions of interest were analyzed, one (16×17 pixels) at the distal femoral metaphysis and one (11×13 pixels) at the distal radius/ulna with a BMD reproducibility (assessed by root mean square coefficient of variation) (RMS-CV) of 4% at the distal femoral metaphysis and 5% at the distal forelimb.

Evaluation of bone microarchitecture by micro-computed tomography

For micro-computed tomographic imaging (microCT), fixed femur or radius/ulnar samples were analyzed using a compact fan-beam-type tomograph (μCT 40, Scanco Medical AG, Bassersdorf, Switzerland). Bone tissues were kept in an airtight cylindrical sample holder filled with formalin. The holders were marked with an axial alignment line to allow for consistent positioning of the specimens. For each sample, approximately 200 micro-tomographic slices with an increment of 17 μm were acquired, covering the entire width of the bone. Three-dimensional analyses were performed to calculate morphometric indices including total volume (TV), bone volume (BV), marrow volume (MV), bone mineral content (BMC), bone surface (BS), bone thickness (Th), and various ratios, including density BV/TV, trabecular thickness [Tb.Th], trabecular number [Tb.N], and trabecular separation [Tb.Sp]. The indices were calculated as previously described [32] with a reproducibility (assessed by precision error) of 0.06–2.16% for the cortical compartment and 0.59–5.24% for the trabecular compartment [33].

Dynamic histomorphometry studies

Sequential injections of calcein, a fluorochrome that incorporates into ossifying bone, were used to mark osteoid deposition and mineralization in vivo. Naïve and severely injured animals were injected i.p. with calcein (10 mg/kg) on day 2 and day 9 post-injury. At 10 days post-injury hindlimbs were resected and dynamic histomorphometric analyses were performed at the distal femoral metaphysis by the Mayo Clinic Histomorphometry Core Laboratory (Rochester, MN).

Goldner’s trichrome staining and trap staining of osteoclast activity

We stained 5 μm deparaffinized bone sections with Goldner’s trichrome method for osteoid identification [34]. Adjacent sections were stained for TRAP to identify mature osteoclasts as previously described [19]. Osteoclasts were counted as TRAP-positive multinucleated cells and the total number was expressed per mm length of growth plate cartilage and mm length of cortical bone.

Results

Rapid decrease in bone mineral density at the femoral metaphysis following SCI

In the experimental group, all animals had severe neurological impairments as evidenced by limited spinal reflexes without functional locomotion. Bone mineral density was assessed by PIXimus scan at the femoral metaphysis (i.e., sublesional skeletal site) and the distal forelimb (skeletal site used as a supralesional control). We found a significant 34% decrease in bone mineral density at the distal femoral metaphysis in the injured animals (n=11) compared to naïve controls (n=9) at 10 days post-injury (0.12±0.02 g/cm^2 versus 0.18±0.02 grams/cm^2, $p<0.001$) (Fig. 1). In contrast, there was no significant difference in the forelimb BMD between the injured and naïve groups (0.09±0.01 grams/cm^2 versus 0.08±0.01 grams/cm^2, $p=0.20$).

Alterations in bone microarchitecture following SCI

MicroCT analysis of the femoral metaphysis revealed a significant alteration in bone microarchitecture due to severe SCI (Fig. 2). We detected an average of 48% decrease in trabecular bone mineral content (Table 1) with an associated decrease in trabecular thickness and connectivity density at the femoral metaphysis in the injured animals (n=5) when compared to the naïve controls (n=5). The mean cortical bone mineral content was also decreased by 35% with significantly decreased cortical thickness. Furthermore, the ratio of bone surface to bone volume (BS/BV (1/mm)) was increased in both compartments indicating increased trabecular and cortical bone resorption.

Increased osteoclast activity following SCI

TRAP staining revealed a statistically significant 333% increase in the number of mature osteoclasts per mm of growth plate in the animals with spinal cord injury (n=3) compared to the naïve controls (n=4). There was no significant change in the number of osteoclasts per mm of cortical bone (Fig. 3a and b).

Alterations in the growth plate and mineral apposition following SCI

Goldner's trichrome staining of adjacent sections demonstrated chrondrocyte disorganization at the growth plate in the injured animals (Fig. 3c). The boundaries between proliferating and hypertrophic zones were less distinct in the injured animals with a loss of both hypertrophic and proliferating chondrocyte columnar alignment. The altered columnar arrangement made chrondrocyte counts per column inaccurate; however we detected a 35% reduction in growth plate width in the injured samples. These changes occur at both the margins and in the center of the growth plate. Appositional growth studies revealed a significantly decreased bone formation rate in the injured animals (Table 2). Additionally, the calcein labeling pattern of ossifying trabecular bone at the distal femoral metaphysis was abnormal only in samples derived from injured animals. In the injured sections the labeling was diffuse with few regions of distinct single or double labeling indicating a mineralization defect (Fig. 4, red arrows). Thus, there appears to be a qualitative and quantitative difference in mineral apposition caused by spinal cord injury.

Discussion

The contusion spinal cord injury model is considered to be the most relevant to clinical SCI and therefore widely used to study the pertinent sequelae of human SCI [35]. In the present study we report a significant decrease in bone mineral density at the distal femoral metaphysis which is associated with markedly reduced bone formation rate, decreased bone mineralization, increased osteoclast activity and disruption of the cellular organization of the growth plate in a rodent model of contusion SCI. These findings indicate that increased bone resorption due to osteoclast activation and decreased bone formation due to an osteoblast defect simultaneously contribute to the pathophysiology of SCI-induced bone loss.

Previously, based on clinical studies of markers of bone turnover, including free and total deoxypyridinoline, total pyridinoline, N-telopeptide, osteocalcin, and total alkaline phosphatase in individuals with spinal cord injury, it was widely assumed that the rapid bone loss following acute SCI is caused by enhanced bone resorption with normal bone formation. Jiang et al. recently reported increased osteoclastic activity from marrow derived precursors following spinal cord transection in rats and concluded osteoclast activity to be more affected than osteoblast activity. They additionally showed increased mineral apposition rate and bone formation rate at 3 weeks post-transection [36]. The seemingly contradictory findings on osteoblasts relative to ours are likely due to differences in the model of experimental spinal cord injury (i.e., transection versus contusion) and the corresponding changes in osteoblast function over time. These findings warrant further investigation of specific osteoblast activities triggered by different modalities of SCI. Our findings are the first to report both osteoclast dysfunction and suppressed osteoblast activity in the development of osteoporosis following lower thoracic contusive spinal cord trauma.

We also noted a loss of normal cellular organization at the growth plate in conjunction with the osteoclast activation and resulting metaphyseal bone loss. This finding suggests that spinal cord injury may result in altered cartilage differentiation and/or signaling between cartilage and growing bone. Children with spinal cord injury are known to have stunted growth of the long bones that are distal to the neurological injury [37]. The growth plate arrest with chondrocyte columnar derangement may represent a histopathogical basis for the growth deficiency seen in human patients. It is also possible that SCI-induced bone loss is greatest in those subjects with immature skeletal bones. This is unlikely as the bone loss that we report is similar in magnitude to that seen in human adults with SCI. However, the impact of gender and skeletal maturity on the severity of SCI-induced osteoporosis needs to be determined in future studies.

We have additionally observed decreased BMD in both the trabecular and cortical compartments. Earlier human studies of BMD by dual-energy X-ray absorptiometry (DXA) reported trabecular bone loss acutely following SCI. A more recent report also showed cortical thinning detected by using peripheral quantitative computed tomography (pQCT) [38]. The trabecular loss is more rapid, but the cortical thinning persists beyond the acute period following SCI. As the mean time to first fracture is 9 years post-injury [39], efforts to slow or prevent the ongoing cortical bone loss are an important therapeutic consideration.

The mechanism of sublesional bone loss following neurological injury is poorly understood. Verhas et al. demonstrated increased bone blood flow at the sites of greatest bone loss in a transection model of SCI and suggested the mechanism of bone loss involves the development of vascular shunts within the bone [40]. Takahashi et al. similarly reported increased regional bone blood flow as early as 6-hours following hemicordotomy with rhizotomy in rats and concluded the spinal nervous system played a role in the control of regional blood flow within the affected bone [41]. Abnormal cytokine levels within the bone have also been implicated in the development of bone loss in sublesional zones. Demulder et al. biopsied bone from the sternum and iliac crest of five neurologically intact volunteers and seven SCI subjects at 6 weeks following spinal cord injury. They reported increased levels of IL-6, a cytokine shown to enhance osteoclast formation and bone resorption, in samples from the SCI patients. They speculated that a local increase of IL-6 in sublesional bones promotes osteoclast recruitment from marrow precursors [42].

A dense network of sensory and sympathetic nerve fibers exists within the marrow, periosteum, cortical and trabecular compartments. Immunohistochemical analysis of rodent long bones has shown neuropeptide expression within these nerve fibers [43]. Neuropeptide surface receptor expression has been described on both osteoclasts and osteoblasts. Receptor activation triggered by neuropep-tide binding causes altered bone cell activity in several in vitro studies [44, 45]. Moreover, nerve fiber distribution has been shown to change in response to neurological injury. Induced sensory and sympathetic denervation dramatically alters the distribution of immunoreactive fibers within rat bone [21, 46]. Neurological injury may result in physiological changes within the bone microenvironment, including shunt formation in blood circulation and changes in cytokine or neuro-osteotrophic factor expression, that ultimately lead to osteoclast activation and osteoblast inhibition.

Our results recapitulate the changes in bone microarchitecture as those detected by peripheral computed tomography following spinal cord injury in humans. Therefore, our work constitutes a foundation offering significant potential for mechanistic studies that are currently lacking and greatly needed to advance the understanding of SCI-induced bone loss. Furthermore, our model and experimental protocols can be readily used to test therapeutic interventions aimed at prevention and amelioration of osteoporosis following neurological injury.

Acknowledgments

We would like to thank Dr. M.van der Vlies and Justine Dobeck for technical assistance and the Swiss National Science Foundation.

Funding Grant sponsor: NIH/NICHD Grant number K12 HD001097-08 (L.M.);

Grant sponsor: VABLR&D121F (Y.D.T.);

Grant sponsor: NIH Grant number R21NS53935 (Y.D.T.);

Grant sponsor: NIH/NICDR Grant number DE007378-18 (P.S.)

References

1. Szollar SM, Martin EM, Sartoris DJ, Parthemore JG, Deftos LJ. Bone mineral density and indexes of bone metabolism in spinal cord injury. Am J Phys Med Rehabil. 1998 Jan; 77(1):28–35. [PubMed: 9482376]
2. Aluisio FV, Scully SP. Acute hematogenous osteomyelitis of a closed fracture with chronic superinfection. Clin Orthop Relat Res. 1996 Apr.325:239–244. [PubMed: 8998882]
3. Cochran TP, Bayley JC, Smith M. Lower extremity fractures in paraplegics: pattern, treatment, and functional results. J Spinal Disord. 1988; 1(3):219–223. [PubMed: 2980141]
4. Garland DE, Saucedo T, Reiser TV. The management of tibial fractures in acute spinal cord injury patients. Clin Orthop Relat Res. 1986 Dec.213:237–240. [PubMed: 3780098]
5. Givre S, Freed HA. Autonomic dysreflexia: a potentially fatal complication of somatic stress in quadriplegics. J Emerg Med. 1989 Sep; 7(5):461–463. [PubMed: 2607106]
6. Watson FM, Whitesides TE Jr. Acute hematogenous osteomyelitis complicating closed fractures. Clin Orthop Relat Res. 1976 Jun.117:296–302. [PubMed: 1277679]
7. Garland DE, Adkins RH, Kushwaha V, Stewart C. Risk factors for osteoporosis at the knee in the spinal cord injury population. J Spinal Cord Med. 2004; 27(3):202–206. [PubMed: 15478520]
8. Warden SJ, Bennell KL, Matthews B, Brown DJ, McMeeken JM, Wark JD. Quantitative ultrasound assessment of acute bone loss following spinal cord injury: a longitudinal pilot study. Osteoporos Int. 2002 Jul; 13(7):586–592. [PubMed: 12111020]
9. Vico L, Collet P, Guignandon A, Lafage-Proust MH, Thomas T, Rehaillia M, Alexandre C. Effects of long-term microgravity exposure on cancellous and cortical weight-bearing bones of cosmonauts. Lancet. 2000 May 6; 355(9215):1607–1611. [PubMed: 10821365]
10. Leblanc AD, Schneider VS, Evans HJ, Engelbretson DA, Krebs JM. Bone mineral loss and recovery after 17 weeks of bed rest. J Bone Miner Res. 1990 Aug; 5(8):843–850. [PubMed: 2239368]
11. Biering-Sorensen F, Bohr HH, Schaadt OP. Longitudinal study of bone mineral content in the lumbar spine, the forearm and the lower extremities after spinal cord injury. Eur J Clin Invest. 1990 Jun; 20(3):330–335. [PubMed: 2114994]
12. Dauty M, Perrouin VB, Maugars Y, Dubois C, Mathe JF. Supralesional and sublesional bone mineral density in spinal cord-injured patients. Bone. 2000 Aug; 27(2):305–309. [PubMed: 10913927]
13. de Bruin ED, Frey-Rindova P, Herzog RE, Dietz V, Dambacher MA, Stussi E. Changes of tibia bone properties after spinal cord injury: effects of early intervention. Arch Phys Med Rehabil. 1999 Feb; 80(2):214–220. [PubMed: 10025500]
14. Demirel G, Yilmaz H, Paker N, Onel S. Osteoporosis after spinal cord injury. Spinal Cord. 1998 Dec; 36(12):822–825. [PubMed: 9881730]
15. Wilmet E, Ismail AA, Heilporn A, Welraeds D, Bergmann P. Longitudinal study of the bone mineral content and of soft tissue composition after spinal cord section. Paraplegia. 1995 Nov; 33(11):674–677. [PubMed: 8584304]
16. Andresen EM, Patrick DL, Carter WB, Malmgren JA. Comparing the performance of health status measures for healthy older adults. J Am Geriatr Soc. 1995 Sep; 43(9):1030–1034. [PubMed: 7657920]
17. Karsenty G. The central regulation of bone remodeling. Trends Endocrinol Metab. 2000 Dec; 11(10):437–439. [PubMed: 11091123]
18. Battaglino R, Fu J, Spate U, Ersoy U, Joe M, Sedaghat L, Stashenko P. Serotonin regulates osteoclast differentiation through its transporter. J Bone Miner Res. 2004 Sep; 19(9):1420–1431. [PubMed: 15312242]
19. Battaglino R, Vokes M, Schulze-Spate U, Sharma A, Graves D, Kohler T, Muller R, Yoganathan S, Stashenko P. Fluoxetine treatment increases trabecular bone formation in mice. J Cell Biochem. 2007 Apr 15; 100(6):1387–1394. [PubMed: 17041947]
20. Cherruau M, Facchinetti P, Baroukh B, Saffar JL. Chemical sympathectomy impairs bone resorption in rats: a role for the sympathetic system on bone metabolism. Bone. 1999 Nov; 25(5): 545–551. [PubMed: 10574574]

21. Cherruau M, Morvan FO, Schirar A, Saffar JL. Chemical sympathectomy-induced changes in TH-, VIP-, and CGRP-immunoreactive fibers in the rat mandible periosteum: influence on bone resorption. J Cell Physiol. 2003 Mar; 194(3):341–348. [PubMed: 12548553]
22. Hill EL, Elde R. Distribution of CGRP-, VIP-, D beta H-, SP-, and NPY-immunoreactive nerves in the periosteum of the rat. Cell Tissue Res. 1991 Jun; 264(3):469–480. [PubMed: 1714353]
23. Hill EL, Turner R, Elde R. Effects of neonatal sympathectomy and capsaicin treatment on bone remodeling in rats. Neuroscience. 1991; 44(3):747–755. [PubMed: 1721689]
24. Nockels R, Young W. Pharmacologic strategies in the treatment of experimental spinal cord injury. J Neurotrauma. 1992 Mar; 9(Suppl 1):S211–S217. [PubMed: 1588610]
25. Thompson MK, Tuma RF, Young WF. The effects of pentoxifylline on spinal cord blood flow after experimental spinal cord injury. J Assoc Acad Minor Phys. 1999; 10(1):23–26. [PubMed: 10826005]
26. Hulsebosch CE, Xu GY, Perez-Polo JR, Westlund KN, Taylor CP, McAdoo DJ. Rodent model of chronic central pain after spinal cord contusion injury and effects of gabapentin. J Neurotrauma. 2000 Dec; 17(12):1205–1217. [PubMed: 11186233]
27. Mills CD, Grady JJ, Hulsebosch CE. Changes in exploratory behavior as a measure of chronic central pain following spinal cord injury. J Neurotrauma. 2001 Oct; 18(10):1091–1105. [PubMed: 11686495]
28. Pikov V, Wrathall JR. Coordination of the bladder detrusor and the external urethral sphincter in a rat model of spinal cord injury: effect of injury severity. J Neurosci. 2001 Jan 15; 21(2):559–569. [PubMed: 11160435]
29. Pikov V, Wrathall JR. Altered glutamate receptor function during recovery of bladder detrusor-external urethral sphincter coordination in a rat model of spinal cord injury. J Pharmacol Exp Ther. 2002 Feb; 300(2):421–427. [PubMed: 11805200]
30. Choi H, Liao WL, Newton KM, Onario RC, King AM, Desilets FC, Woodard EJ, Eichler ME, Frontera WR, Sabharwal S, Teng YD. Respiratory abnormalities resulting from midcervical spinal cord injury and their reversal by serotonin 1A agonists in conscious rats. J Neurosci. 2005 May 4; 25(18):4550–4559. [PubMed: 15872102]
31. Teng YD, Lavik EB, Qu X, Park KI, Ourednik J, Zurakowski D, Langer R, Snyder EY. Functional recovery following traumatic spinal cord injury mediated by a unique polymer scaffold seeded with neural stem cells. Proc Natl Acad Sci USA. 2002 Mar 5; 99(5):3024–3029. [PubMed: 11867737]
32. Ruegsegger P, Koller B, Muller R. A microtomographic system for the nondestructive evaluation of bone architecture. Calcif Tissue Int. 1996 Jan; 58(1):24–29. [PubMed: 8825235]
33. Kohler T, Beyeler M, Webster D, Muller R. Compartmental bone morphometry in the mouse femur: reproducibility and resolution dependence of microtomographic measurements. Calcif Tissue Int. 2005 Nov; 77(5):281–290. [PubMed: 16283571]
34. Villanueva AR, Mehr LA. Modifications of the Goldner and Gomori one-step trichrome stains for plastic-embedded thin sections of bone. Am J Med Technol. 1977 Jun; 43(6):536–538. [PubMed: 69401]
35. Dietz V, Curt A. Neurological aspects of spinal-cord repair: promises and challenges. Lancet Neurol. 2006 Aug; 5(8):688–694. [PubMed: 16857574]
36. Jiang SD, Jiang LS, Dai LY. Effects of spinal cord injury on osteoblastogenesis, osteoclastogenesis and gene expression profiling in osteoblasts in young rats. Osteoporos Int. 2007 Mar; 18(3):339–349. [PubMed: 17036173]
37. Duval-Beaupere G, Lougovoy J, Trocellier L, Lacert P. Trunk and leg growth in children with paraplegia caused by spinal cord injury. Paraplegia. 1983 Dec; 21(6):339–350. [PubMed: 6664685]
38. Eser P, Schiessl H, Willnecker J. Bone loss and steady state after spinal cord injury: a cross-sectional study using pQCT. J Musculoskelet Neuronal Interact. 2004 Jun; 4(2):197–198. [PubMed: 15615125]
39. Eser P, Frotzler A, Zehnder Y, Schiessl H, Denoth J. Assessment of anthropometric, systemic, and lifestyle factors influencing bone status in the legs of spinal cord injured individuals. Osteoporos Int. 2005 Jan; 16(1):26–34. [PubMed: 15138665]

40. Verhas M, Martinello Y, Mone M, Heilporn A, Bergmann P, Tricot A, Schoutens A. Demineralization and pathological physiology of the skeleton in paraplegic rats. Calcif Tissue Int. 1980; 30(1):83–90. [PubMed: 6767536]

41. Takahashi H, Yamamuro T, Okumura H, Kasai R, Tada K. Bone blood flow after spinal paralysis in the rat. J Orthop Res. 1990 May; 8(3):393–400. [PubMed: 2324858]

42. Demulder A, Guns M, Ismail A, Wilmet E, Fondu P, Bergmann P. Increased osteoclast-like cells formation in long-term bone marrow cultures from patients with a spinal cord injury. Calcif Tissue Int. 1998 Nov; 63(5):396–400. [PubMed: 9799824]

43. Serre CM, Farlay D, Delmas PD, Chenu C. Evidence for a dense and intimate innervation of the bone tissue, including glutamate-containing fibers. Bone. 1999 Dec; 25(6):623–629. [PubMed: 10593406]

44. Chenu C. Glutamatergic regulation of bone resorption. J Musculoskelet Neuronal Interact. 2002 Sep; 2(5):423–431. [PubMed: 15758410]

45. Lundberg P, Lerner UH. Expression and regulatory role of receptors for vasoactive intestinal peptide in bone cells. Microsc Res Tech. 2002 Jul 15; 58(2):98–103. [PubMed: 12203709]

46. Adam C, Llorens A, Baroukh B, Cherruau M, Saffar JL. Effects of capsaicin-induced sensory denervation on osteoclastic resorption in adult rats. Exp Physiol. 2000 Jan; 85(1):62–66. [PubMed: 10662894]

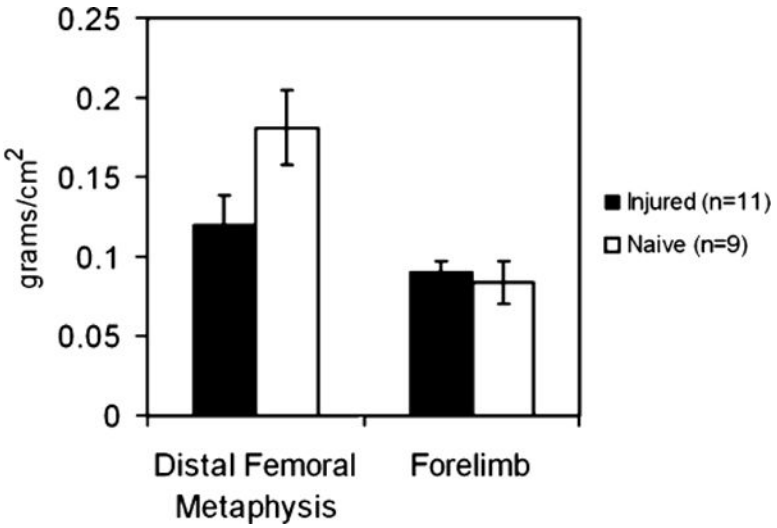

Fig. 1.

Rapid post-SCI decrease of mineral density in bones innervated by spinal cord segments caudal to the injury epicenter. Bone mineral density was determined ten days post-injury at the distal femoral metaphysis in spinal cord injured and naïve rats by PIXImus. The forelimb was used as a supralesional control. There was a significant loss in average bone mineral density at the distal femoral metaphysis in the spinal cord injured group (34%). No change in bone mineral density was found at the forelimb site

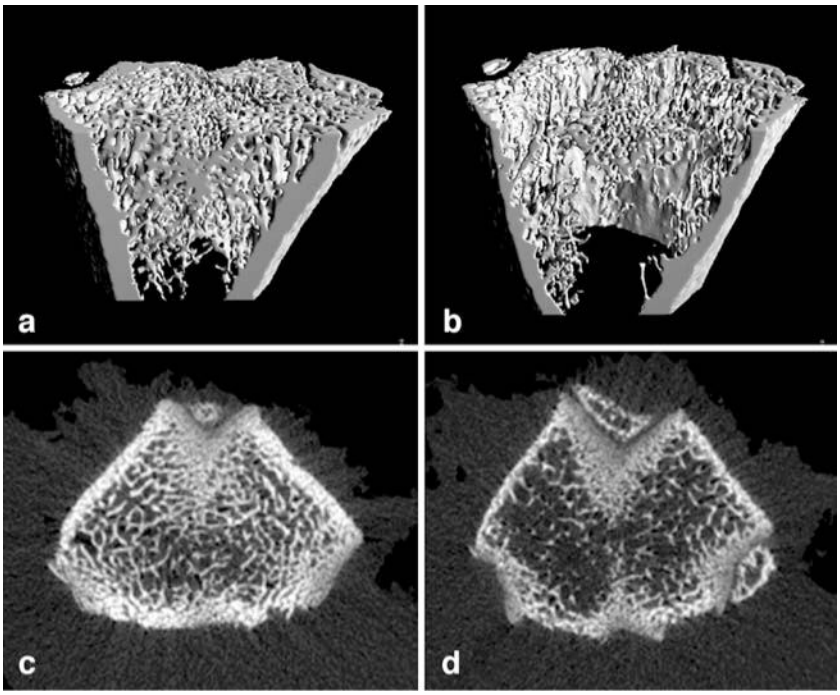

Fig. 2.

Rapid decrease in trabecular and cortical bone following SCI. Three-dimensional (panels **a** and **b**) and two dimensional (panels **c** and **d**) microCT reconstruction of the trabecular bone component of the distal femoral metaphysis in naive (left) and SCI (right) rats. The SCI rats display a marked decrease in trabecular bone volume and cortical thickness (see Table 1 for details)

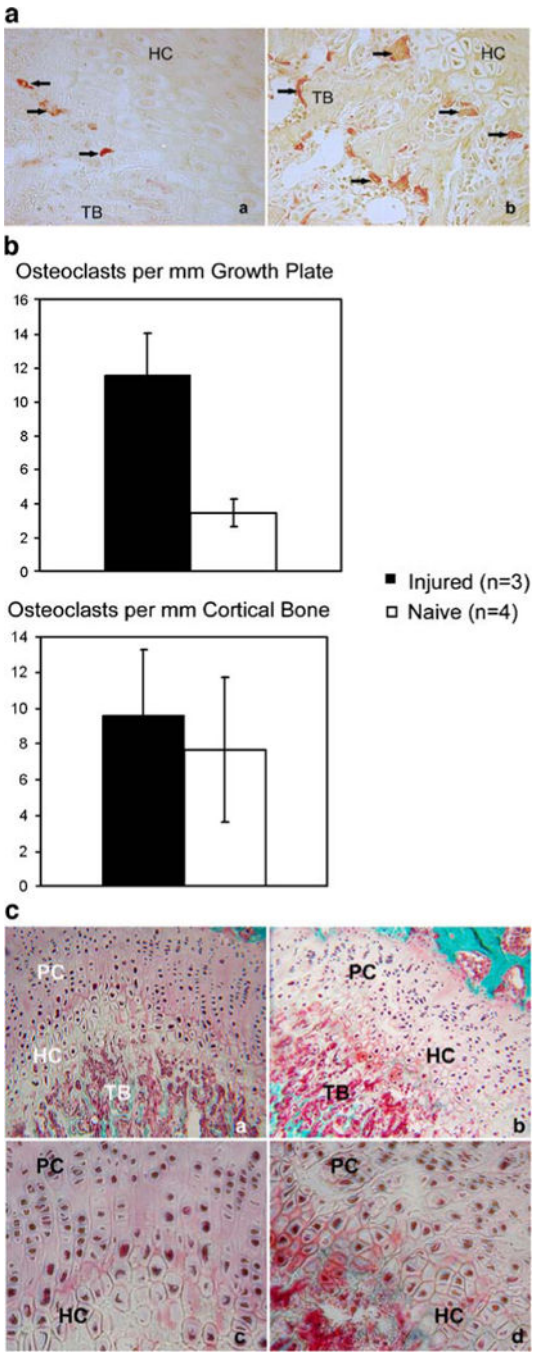

Fig. 3.

SCI-induced osteoclast activation and growth plate disorganization. Bone sections through the knee joint of naïve control (3**a**, panel **a**) and injured rats (3**a**, panel **b**) were TRAP stained to identify mature osteoclasts. Arrows indicate TRAP positive cells. Trabecular bone (TB) and hypertrophic chrondrocytes (HC) are indicated at the growth plate. The injured animals had 330% more TRAP positive cells at the growth plate (Fig. 3b top) with no change in cortical TRAP positive cells (Fig. 3b, bottom). Goldner's trichrome staining of adjacent sections demonstrates normal cellular arrangement at the growth plate in the naive

animals (Fig. 3c panels **a** and **c**) and cellular disorganization in the injured animals (Fig. 3c panels **b** and **d**)

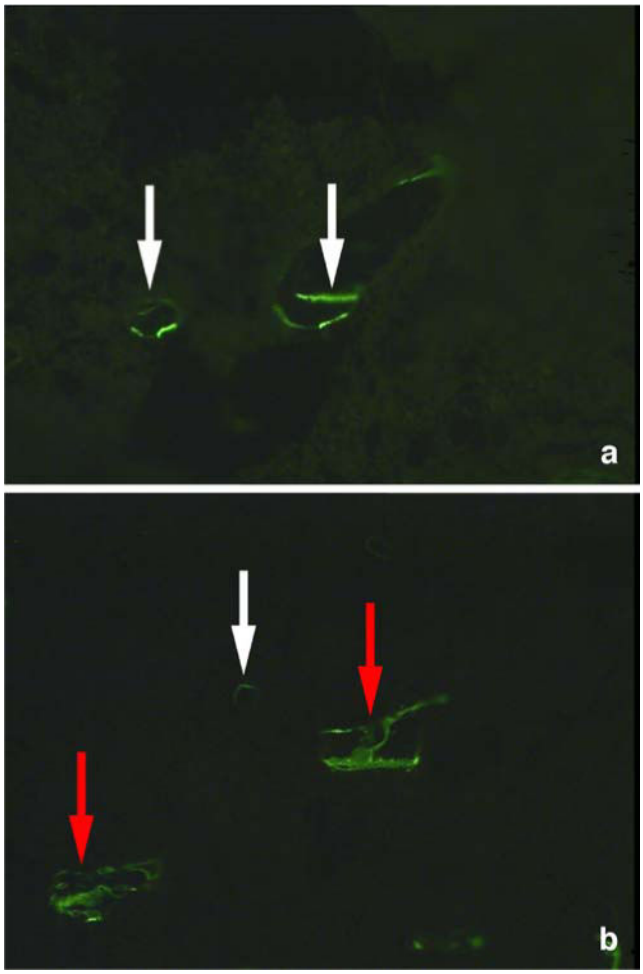

Fig. 4.

SCI-induced mineralization defect. Dynamic histomorphometry was performed at the trabecular surface of the distal femoral metaphysis following injection of calcein, a marker of osteoid deposition and mineralization in vivo. Normal double labeling was seen in the control animals (**a**, white arrow). In the SCI group, labeling was abnormal (**b**, red arrow) indicative of a mineralization defect with limited normal double labeling (**b**, white arrow)

Table 1

Analysis of bone microarchitecture at the distal femoral metaphysis by microCT

	Naïve (n=5)	Injured (n=5)
Trabecular parameters (sd)		
Total volume (TV) (mm^3)	30.92(2.21)	42.56(3.41)***
Bone volume (BV) (mm^3)	3.26(0.30)	1.70(0.88)*
Bone mineral content (BMC) (mg)	5.83(0.53)	3.04(1.57)*
Bone surface (BS) (mm^2)	128.05(12.22)	81.71(37.63)
BV/TV (%)	10.55(0.94)	4.06(2.25)**
BS/TV(mm^2/mm^3)	4.14(0.30)	1.95(0.96)*
BS/BV(mm^2/mm^3)	39.34(2.16)	49.32(3.43)**
Trabecular thickness (Tb. Th) (mm)	0.08(0.003)	0.06(0.004)**
Tb. spacing (Sp.) (mm)	0.74(0.08)	1.00(0.31)
Tb. number (N) (1/mm)	1.43(0.16)	1.09(0.31)
Connectivity density ($1/mm^3$)	36.33(3.64)	6.11(5.69)***
Cortical parameters (sd)		
TV (mm^3)	19.61(1.28)	20.83(0.76)
Marrow volume (MV) (mm^3)	12.78(1.34)	15.83(1.07)**
BMC (mg)	12.22(0.47)	8.94(1.48)*
BV	6.83(0.3)	5.00(0.8)*
BS (mm^2)	32.29(3.81)	34.48(3.11)
BV/TV (%)	34.94(2.77)	24.01(4.01)**
BS/TV (1/mm)	1.65(0.18)	1.66(0.20)
BS/BV (1/mm)	4.74(0.66)	7.08(1.50)*
MV/TV (%)	65.06(2.77)	75.99(4.01)**
Cortical thickness (Ct. Th) (mm)	0.36(0.03)	0.25(0.03)**

* indicates $p \leq 0.05$

** indicates $p \leq 0.005$

*** indicates $p \leq 0.0005$

Table 2

Dynamic histomorphometry at the distal femoral metaphysis

	Naïve (n=4)	Injured (n=7)
Dynamic histomorphometry (sd)		
Total area (TA)	3.20(0.35)	3.32(0.79)
Marrow surface/Bone surface	7.96(3.93)	3.20(2.03)*
Mineralization appositional rate	2.12(0.94)	1.70(0.19)
Bone formation rate/Bone surface	69.24(43.57)	19.79(13.32)*
Bone formation rate/Bone volume	319.84(226.28)	92.74(69.78)*

* indicates p≤0.05